Geomagnetically Induced Current Modeling in New Zealand: Extreme Storm analysis using multiple disturbance scenarios and industry provided hazard magnitudes

D. H. Mac Manus[1], C. J. Rodger[1], M. Dalzell[2], A. Renton[2], G. S. Richardson[3], T. Petersen[4], and M. A. Clilverd[5]

[1]Department of Physics, University of Otago, Dunedin, New Zealand.
[2]Transpower New Zealand Ltd., Wellington, New Zealand.
[3]British Geological Survey (UKRI-NERC), Edinburgh, UK.
[4]GNS Science, Wellington, New Zealand.
[5]British Antarctic Survey (UKRI-NERC), Cambridge, UK.

Key Points:

- Magnetic fields from large geomagnetic events imposed with different latitude variations can produce theoretical extreme storm scenarios.
- Extreme storm scenarios consistently predict between 13-35% of New Zealand transformers reaching dangerous levels of long lasting GIC.
- The transformers at most risk of long lasting GIC are not confined to a small region, instead spread throughout the length of New Zealand.

Corresponding author: Daniel Mac Manus, macda381@student.otago.ac.nz

Abstract

Geomagnetically induced currents (GICs) are induced in electrical power transmission networks during geomagnetic disturbances. Understanding the magnitude and duration of the GIC expected during worst-case extreme storm scenarios is vital to estimate potential damages and disruptions to power networks. In this study we utilize the magnetic field waveforms measured during three large geomagnetic storms and scale them to expected worst case extreme storm magnitudes. Multiple methods are used to simulate the varying magnitude of the magnetic field across the different latitudes of New Zealand. Modeled GIC is produced for nine extreme storm scenarios, each covering 1-1.5 days in duration. Our industry partners, Transpower New Zealand Ltd provided GIC magnitude and duration levels which represent a risk to their transformers. Using these thresholds various extreme storm scenarios predict between 44 and 115 New Zealand transformers (13-35%) are at risk of damaging levels of GIC. The transformers at risk are largely independent of the extreme storm time-variations, but depend more on the latitude variation scenario. We show that these at-risk transformers are not localized to any specific region of New Zealand but extend across all regions and include most of the major population centers. A peak mean absolute GIC over a 60-minute window of 920-2210 A and an instantaneous one-minute time resolution maximum GIC of 1590-4920 A occurs for a worst-case extreme storm scenario. We believe this is one of the first studies to combine a reasonable worst-case extreme geomagnetic storm with validated GIC modeling and industry-provided GIC risk thresholds.

Plain Language Summary

Space Weather events can cause unwanted DC currents in electrical power transmission networks during geomagnetic storms. We model multiple difference extreme storms to determine the worst case DC currents expected. We work with our industry partners in New Zealand to determine DC magnitudes and durations that would put different types of transformers at risk. Using these values we predict multiple transformers are at risk of damaging levels of DC current. We show that the transformers at risk are located throughout all regions of New Zealand. We believe this is one of the first studies that combines multiple extreme storms scenarios with industry provided DC current magnitudes and durations to determine the risk to transformers.

1 Introduction

Geoelectric fields, E, are induced in the conducting Earth as a result of rapid, large magnetic field variations due to space weather activity. Furthermore, the induced E-fields lead to Geomagnetically Induced Currents (GIC) flowing through grounded conducting structures such as pipelines, railways and high-voltage electrical transmission grids (Bolduc, 2002). It is the latter for which we are concerned about in this study. The generation, transmission and distribution of electricity is an essential lifeline utility service for a modern society. Any disruption to power systems is of major concern.

Geomagnetic field disturbances, specifically local, large horizontal field component rates of change, *H'* are a good indicator of induced electric field (Cagniard, 1953). This in turn is the primary driver of large GIC (Viljanen et al., 2001). Mac Manus et al. (2017) utilised ∼14 years of GIC measurements from multiple transformers in New Zealand and compared them with various geomagnetic field components, finding the majority of transformers correlating with *H'*. Large *H'* usually occurs at the sudden commencement phase of a geomagnetic storm but can also occur throughout the storm main phase or as a result of substorms occurring during the storm. The largest measured *H'* to date is ∼2700 nT/min, recorded at the Lovo observatory (55.8° corrected geomagnetic latitude) near Stockholm Sweden in July 1982 (Kappenman, 2006). This led to maximum geoelectric fields of 9.1 V/km. Kappenman (2004) noted that electric fields of ∼20 V/km occurred

in that same region during the extreme May 1921 geomagnetic disturbance, indicating a peak rate of change of 4000 nT/min is possible. Thomson et al. (2011) used extreme value statistics and 1-minute data from European magnetic observatories over a 30 year period to examine extreme storm *H'*. For geomagnetic latitudes of the United Kingdom (UK) the worst case scenario, indicated by the upper limit of the 95% confidence interval gives a predicted *H'* of 4000 nT/min for a one hundred year return period (increasing to 6000 nT/min for two hundred year return). Similar levels are given for a "reasonable worst-case scenario" in the UK of 5000 nT/min (Cannon, 2013). For contrast, the largest measured *H'* in the UK to date is 1100 nT/min in 1991 (Beggan et al., 2013).

The probability of such worst-case scenarios occurring has been examined in many studies. Love (2012) used Poisson occurrence probability to show a 10 year return period for a Carrington level event of 6.3%. Other statistical approaches have found this likelihood ranging from anywhere as low as 3% up to 12% (Cannon, 2013; Chapman et al., 2020; Riley, 2012; Riley & Love, 2017).

The impact of the Carrington event in 1859 was comparatively minimal, in terms of technological disruption and damage. Telegraph lines connecting Boston and Portland in the USA operated for over an hour "with the aid of celestial batteries alone" (Kappenman & Albertson, 1990). To the best of our knowledge the negative influence of the Carrington event on ground-based infrastructure was limited to telegraph systems. No grounded power network systems existed at the time of the Carrington event. Given our present day reliance on such technology, a magnetic storm of similar magnitude occurring today would likely have a much more widespread and damaging impact (National Research Council, 2008). Multiple power networks around the world could simultaneously be disrupted or damaged.

Various studies discussed in the following paragraphs have estimated the economic cost of a catastrophic GIC event. This goes far beyond just the expected damage to expensive transformer infrastructure and includes the effects of a large electrical blackout on essentials such as food and water supplies as well as disruptions to valuable services like health and transport networks. Major power grid transformers are typically built to order and come in a range of different sizes and configurations. A space weather event that destroys a large number of these transformers could require months to fully repair or replace, perhaps longer. The damage or permanent removal of a power transmission asset can hinder the ability to correctly restore the electricity supply until a spare or replacement asset is provided. The United States National Academy of Sciences (National Research Council, 2008) found that an extreme geomagnetic storm could destroy upwards of 300 of the 2100 high voltage transformers in the U.S electric grid. It is highly likely that this number has decreased with increased research in transformer protection over the past decade however we are unable to find a newer estimate for this value. Replacement transformers would likely cost multi-millions and take many years to manufacture and install.

A long-lasting electrical blackout in one region of the world is likely to have effects on the rest of the globe, due to the strongly connected global economy. Oughton et al. (2017) estimated that following an extreme space weather event the direct economic cost caused by disruption to electrical supply would be only 49% of the total macroeconomic cost, with the rest being attributed to the inevitable disruption to global supply chains. The estimated costs are immense; Lloyd's of London (Lloyd, 2013) estimated that a scenario where 20-40 million people are without power for 16 days to two years could cost \$0.6-2.6 trillion USD.

In this study we investigate the GIC expected in New Zealand for a worst-case extreme geomagnetic storm intended to be on the order of the 1859 Carrington event. We use multiple different time varying geomagnetic field variation scenarios as the model input, to represent uncertainties in the variability during an extreme storm. We combine

this with multiple different geomagnetic latitude variations to simulate the variation in the magnetic field across the transmission network. Our national grid partners have provided us with various different "danger threshold" levels of mean induced currents averaged across given time periods. These hazard magnitudes vary depending on the type of transformer, which our partners have also helped us identify. This allows us to better determine the risk to individual transformers across the New Zealand electrical network during an extreme storm. We show that there are reoccurring transformers at substations with large GIC, indicating regions where mitigation efforts should be focused in a future study. We find that these hotspot locations range across the entire length of New Zealand, but are fairly consistent across the different storm scenarios. We believe the provision of mean GIC hazard levels by our industry partners is a world first and note that these transformer hazard magnitudes should not be specific to New Zealand, and are likely valid globally.

2 Extreme Storm Scenarios

To derive some possible extreme storm scenarios we need to consider a number of characteristics of a severe geomagnetic disturbance. These primarily consist of two factors: the geomagnetic field time series and the geomagnetic latitude variation. These characteristics will be explained in more detail below in Sections 2.1 and 2.2.

2.1 Geomagnetic time series

Due to the lack of observational information about extreme events on the order of the Carrington storm we do not know what the geomagnetic time series would look like. While measurements were made during the Carrington event, they are complicated by the limitations of the equipment of that era, with faint traces, out of range values, and poor experimental response speed. Therefore we will look at several more modern time series that we use to represent the potential variability of an extreme storm as a function of time. Using the time series of past geomagnetic events we then scale them to the expected maximum magnetic field rate of change.

This approach is justified when considering the geospace drivers that produced these past geomagnetic field signatures. Pulkkinen et al. (2012) described how many different dynamic processes are involved in generating the magnetic field including the interactions of the solar wind with the magnetosphere and ionosphere systems. Each step along this process has its own unique complex characteristics and no single geomagnetic time series is capable of capturing the full variation of extreme storms. By using past observed storms we hope to also accurately capture the variations occurring throughout the whole duration of a storm. The importance of this from a GIC standpoint will be addressed in a later section, but we note that the long duration of enhanced GIC can have different technological implications when compared to the short-duration maximum GIC often seen at the sudden commencement. Weigel and Baker (2003) showed one can view the solar wind input as effectively a linear amplifier of the ground magnetic field fluctuations. Consequently by taking an observed geomagnetic field storm one can scale it to represent larger solar wind driving conditions, while maintaining the temporal structure of the magnetic field variations.

The geomagnetic observatory in New Zealand is located at Eyrewell (EYR) (43.474° S, 172.393° E; blue hexagon in Figure 2 of Mac Manus et al. (2022)). It is part of INTERMAGNET (https://intermagnet.github.io/) and is operated by GNS Science, New Zealand. This station provides 1-minute (and more recently 1-second) magnetic field data of various coordinates with 0.1 nT resolution. In one of our scenarios outlined below we use observations from the Ottawa (OTT) magnetic observatory in Canada (45.403° N, 284.448° E), which is also part of INTERMAGNET.

For our extreme storm scenarios we have selected the geomagnetic field fluctuations from three large geomagnetic storm events that have occurred in the past: 13-14 March 1989, 29-30 October 2003 and 7-8 September 2017. These are described in more detail below.

2.1.1 March 1989

The March 1989 storm caused the collapse of the Hydro Quebec high voltage power transmission system (Kappenman & Albertson, 1990; Boteler, 2019). This storm was driven by two large coronal mass ejections (CME), which are known to be significant drivers of GIC (Huttunen et al., 2008). The second sudden storm commencement at 07:43 UT on 13th March occurred at the same time as the substorm that impacted Hydro-Quebec. This lead to the large GIC that caused the Hydro-Quebec collapse (Boteler, 2019). The largest ever recorded Dst index of -589 nT was recorded during the main phase of this storm. Due to the lack of Eyrewell magnetic field measurements for this event we have used the magnetic field time series from the Ottawa (OTT) magnetic observatory. These measurements consist of 1866 minutes of magnetic field fluctuations beginning at 00:00 UT on 13th March 1989 (i.e., roughly 1.3 days). A Maximum *H'* of ∼550 nT/min was measured during this event (Oughton et al., 2017), although the 07:43 UT collapse was associated with an earlier and smaller *H'* increase of 390 nT/min.

2.1.2 October 2003

The October 2003 storm caused blackouts in Southern Sweden (Pulkkinen et al., 2005) and might have contributed to transformer failure in the South African high-voltage transmission system (Gaunt & Coetzee, 2007). Like March 1989, this storm was also driven by a CME and a Dst index of -383 nT was recorded. The magnetic field time series from Eyrewell was used for this event and consists of 2048 minutes beginning at 00:00 UT on 29th October 2003. A maximum *H'* of ∼170 nT/min was measured at 06:11 UT on 29th October 2003.

2.1.3 September 2017

The September 2017 storm was caused by two CMEs in quick succession impacting the magnetosphere. The magnetic field time series for this event consists of 1440 minutes beginning at 20:00 UT on 7th September 2017 from the Eyrewell magnetometer. This event has been discussed extensively by (Clilverd et al., 2018, 2021) and is characterised by two separate intervals of geomagnetic disturbance, each lasting around six hours. A maximum *H'* of ∼40 nT/min was measured at 23:02 UT on the 7th September.

2.1.4 Time series scaling

These three time series selected represent some of the largest events in recent history. However, these disturbances need to be scaled up to a magnitude expected for a worst-case extreme geomagnetic storm. As previously mentioned Thomson et al. (2011) estimated that for UK geomagnetic latitudes the upper limit of the 95% confidence interval gives a predicted *H'* of 4000 nT/min for a one hundred year return period (increasing to 6000 nT/min for two hundred year return). Looking at the corrected geomagnetic latitude (CGM) of the UK we note that they lie at very similar latitudes to New Zealand. The cities of London and Edinburgh in the UK are at comparable geomagnetic latitudes to the cities of Wellington and Dunedin in New Zealand. Due to these latitudinal similarities we believe it is appropriate to use the UK *H'* extreme storm predictions for New Zealand. For the purpose of this study we have decided to use the upper limit for a one hundred year return period of 4000 nT/min. We note this is broadly consistent with the

updated UK space weather worst-case environment report, which suggests a peak of 5000 nT/min (Hapgood et al., 2020).

The three time series have therefore been scaled such that their maximum *H'* is 4000 nT/min. For the September 2017 storm this requires a scaling factor of 100 while for October 2003 it is ∼25. The March 1989 Hydro Quebec event has been scaled by approximately seven. These three scaled time series are shown in Figure 1.

For magnetic field observations, the time series recorded at a geomagnetic observatory is the ground-based magnetic field at that specific location. Likewise, once a geomagnetic field time series has been defined, such as those shown in Figure 1, it is only valid for the geomagnetic latitude that it was derived for. For the purposes of this study we have assigned these time series as if they were to occur at the location of the Eyrewell magnetometer (-50.1° CGM). We acknowledge that this selection is rather arbitrary but it is worth noting that extreme storm predictions for *H'* are not given at a specific location but rather for a range of geomagnetic latitudes (Thomson et al., 2011).

2.2 Latitude variations

To utilise our extreme magnetic field time series scenarios at other locations across New Zealand, we should scale it to account for the expected regional differences based on geomagnetic latitude. Geomagnetic latitude is defined in a similar way to geographic latitude except it is in relation to the magnetic poles instead of the geographic poles. The ground magnetic field signature is dominated by different magnetosphere-ionosphere source currents at different geomagnetic latitudes. At low latitudes a combination of multiple sources such as ring equatorial electrojet, magnetotail and magnetopause currents are responsible for the ground magnetic field signature, while at high latitudes it is primarily driven by auroral ionospheric currents (Kivelson & Russell, 1995; Gombosi, 1998; Ohtani et al., 2000). Geomagnetic activity can often be expressed as a function of geomagnetic latitude.

Various studies have analyzed magnetic field data from multiple stations worldwide to show latitude profiles for large geomagnetic storms. Love et al. (2016) looked at 34 magnetometers around the world and found a sharp peak in *H'* at 60°. In contrast Pulkkinen et al. (2012) looked at the March 1989 and October 2003 events and suggested *H'* peaked in a latitude band around 50-55°, below which *H'* drops off rapidly. This was supported by Ngwira et al. (2013) for 12 large geomagnetic storms. Rogers et al. (2020) fitted Generalised Pareto (GP) distributions to 1-minute measurements of *H'* from 125 magnetometers with an average of 28 years of data per site. With this, latitude fits from 0-90° were predicted for return periods between five and 500 years. A sharp peak is found at 53° in both hemispheres and "no significant hemispherical differences in the CGM latitude profiles" exist, broadly agreeing with the previous studies mentioned and supporting the use of northern hemisphere extreme storm predictions (such as the UK) in Southern hemisphere countries of similar latitudes like New Zealand.

In this study we have applied two different geomagnetic latitude variations as well as applying a constant magnetic field across the whole country explained in more detail in the following sections. Hence each of our three extreme storm time varying scenarios also has three different magnetic field variation scenarios.

2.2.1 NERC scale

The North American Electric Reliability Corporation (NERC) looked at defining a benchmark geomagnetic disturbance representing a low frequency, high impact event (NERC, 2016). The benchmark geomagnetic disturbance event was defined at 60°. In that study a geomagnetic latitude variation scaling approach was used to reduce the magnitude of geomagnetic activity as you move away from the Earth's magnetic poles. This

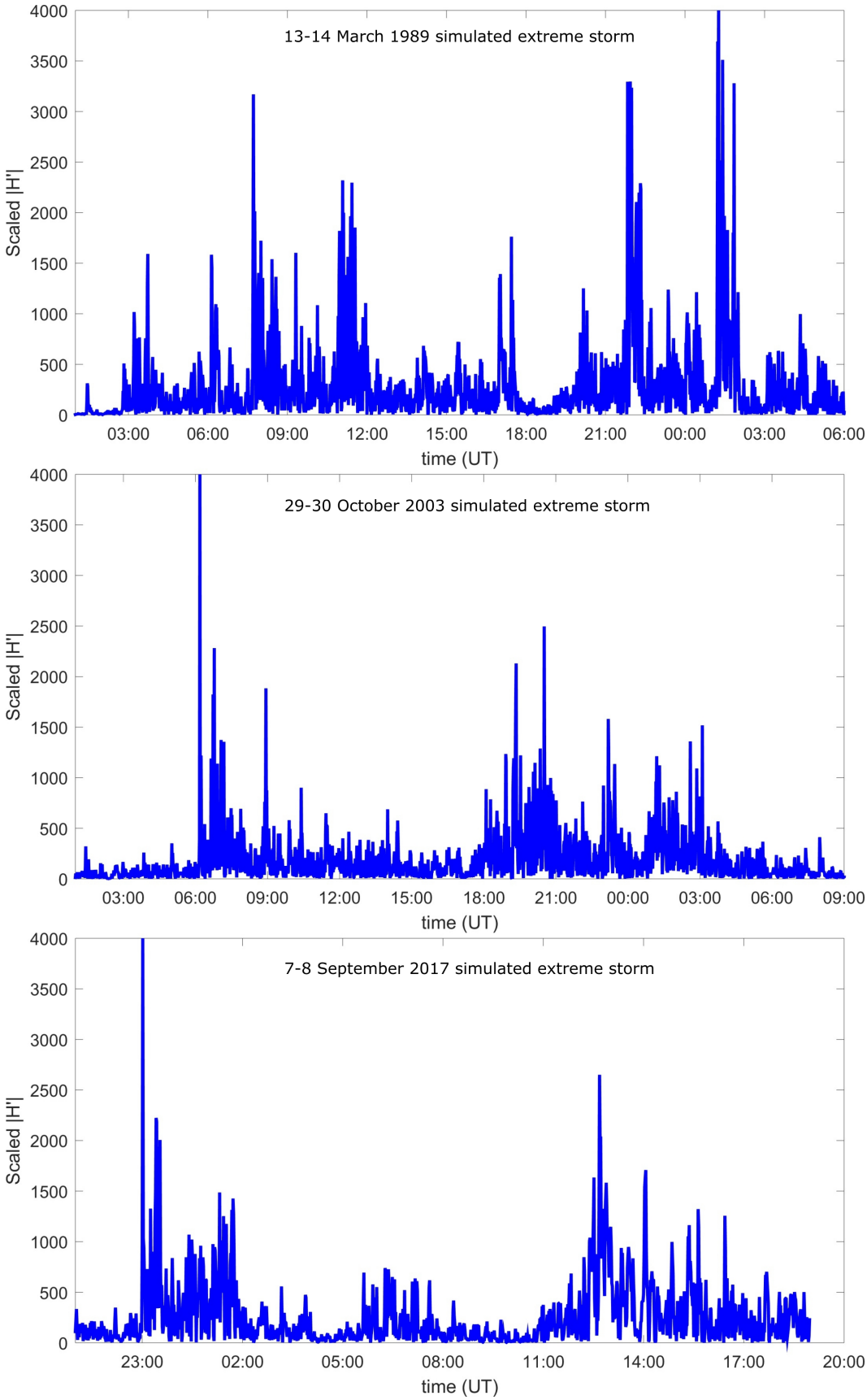

Figure 1: The three simulated extreme storms based on past observed and large geomagnetic events. Each storm has its maximum *H'* scaled up to 4000 nT/min, following estimates of the extreme storm peak expected from the literature.

latitude scaling factor was obtained from the studies of Thomson et al. (2011), Pulkkinen et al. (2012), and Ngwira et al. (2013) and approximated as the expression given in equation 1,

$$\alpha = 0.001 * e^{-0.115*L}, \quad (1)$$

where L is the geomagnetic latitude in degrees (valid between 40 and 60°) and α represents the scale relative to the reference latitude of 60°.

2.2.2 ROGERS scale

As previously mentioned, Rogers et al. (2020) predicated various return levels for return periods of geomagnetic field fluctuations between five and 500 years. Fig. 4 of Rogers et al. (2020) shows the return levels of *H'* for return periods of 100, 200, and 500 years along with fitted smoothed splines for return periods of 5-500 years in panel (d). The authors kindly provided the $MATLAB^{TM}$ scripts used to generate these spline curves in the Supplementary Material. For the purposes of our study we have chosen to use the spline fit for a 500 year return period, given this should be "very extreme". This will be referred to as "ROGERS scale" from this point on. For the most extreme worst-case scenarios an equatorward expansion of the Auroral Electrojet towards lower geomagnetic latitudes is expected (Ahn et al., 2005).

2.2.3 Comparison

For both latitude variations we have normalised the fits such that the maximum *H'* at Eyrewell is 4000 nT/min. The differences in the two latitude variations affect the magnitude of *H'* for the different regions of New Zealand. As shown in Figure 2 the maximum *H'* for the NERC latitude scale is larger at the two ends of New Zealand (shown by the black stars in Figure 2). This shows how significant the geomagnetic latitude variation is to the magnetic field strength as it varies from ∼1600 nT/min (∼700 nT/min for ROGERS scale) at -41° to ∼6100 nT/min (∼5600 nT/min) at -55°.

Figure 3 shows the latitude variation as a simple line plot. Here we can more clearly see that the gradient for the ROGERS scale drops off more rapidly for the lower latitudes (regions north of Eyrewell), before smoothing out gradually below 44°. The NERC scale follows an exponential fit, hence by normalising the results at Eyrewell we find a region between 50.1 and 53.5° for which the ROGERS scale produces larger *H'*. This encloses a region between Eyrewell and the city of Dunedin.

2.2.4 Constant magnetic field

Scenarios with a spatially uniform magnetic field equal to those defined in section 2.1 and shown in Figure 1 are also applied to the whole region of New Zealand. Clearly, this gives large *H'* for regions north of Eyrewell and smaller *H'* for those south of Eyrewell when compared with the two geomagnetic field latitude variations discussed in Sections 2.2.1 and 2.2.2 and shown graphically in Figure 3.

This leaves us with nine different extreme storms scenarios (three magnetic time series and three geomagnetic field latitude variations). Each of these magnetic field signatures differs from each other and provides reasonable assurance that we are covering a wide variation in the range of potential extreme storms that may impact the Earth in the future.

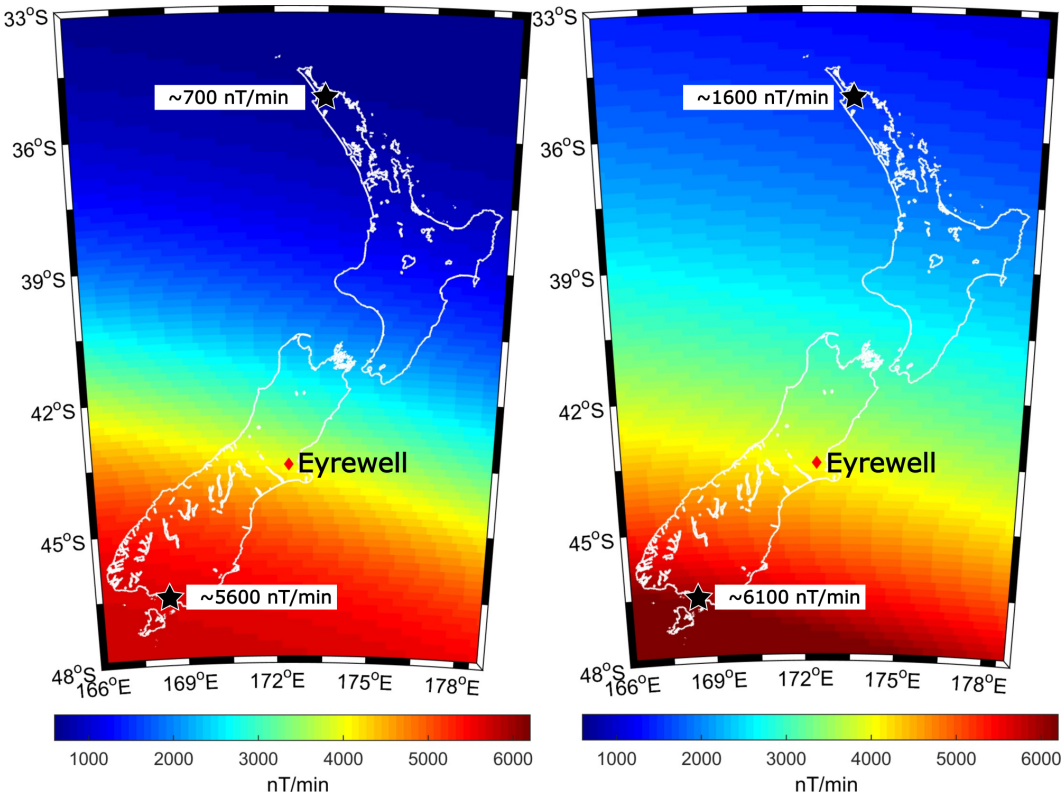

Figure 2: Colour plot showing the maximum *H'* for the ROGERS (left) and NERC (right) latitude variations. The location of the Eyrewell magnetometer is given by the red diamond and represents the location for which both variations have been set to 4000 nT/min. The black stars provide data on levels at the northern-most and southern-most tips of the main islands.

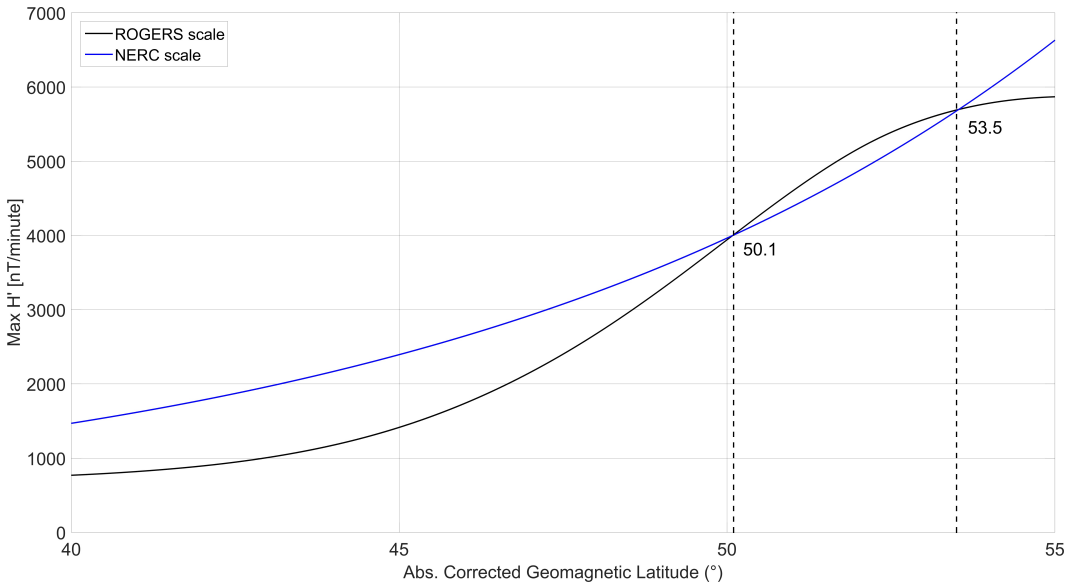

Figure 3: Simplified line representation of Figure 2 showing the maximum *H'* for the ROGERS (black) and NERC (blue) latitude variations. The black dotted lines indicate the region for which the ROGERS scale is larger.

3 Modeling Method

Many studies modeling GIC in New Zealand have been carried out over the years. These studies primarily use the thin sheet model (Divett et al., 2017, 2018, 2020; Mac Manus et al., 2022). These studies have utilised a large spatially varying set of GIC observations to validate the model against. Rodger et al. (2020) showed significant agreement between Total Harmonic Distortion (THD) and model GIC output in the South Island and highlights potential areas of concern in the North Island for locations where GIC observations are not currently taken. Ingham et al. (2017) used MT measurements in New Zealand to create transfer functions that predict GIC at a number of key transformers in the South Island of New Zealand during geomagnetic storms. Mukhtar et al. (2020) was able to use MT measurements to calculate GIC in the North Island, confirming high currents in transformers where THD increases were reported by Rodger et al. (2020).

The approach used in this study is a thin sheet model similar to that explained in Section 2 of Mac Manus et al. (2022). Here, we will give a short summary of each subsection and address any areas which differ to that study.

3.1 Ground Conductance Model

A thin-sheet conductance (TSC) model of New Zealand and the surrounding ocean is used to calculate the electric field. The TSC modeling technique was developed by Vasseur and Weidelt (1977). One sixth of a degree (roughly 20 km) grid cells exist with the integrated conductance of the upper 20 km of crust representing the on-land conductance of each cell. The underlying structure is represented as four layers with resistivity of 1,000, 10,000, 100, and 1 Ω/m at layer boundaries of 20, 60, and 320 km depths.

3.2 Geomagnetic Field

The geomagnetic field input are the nine different extreme storm scenarios explained in section 2. These are of 1-minute cadence at a resolution of 0.1 nT. The X (positive to geographic north, and Y (positive toward east) components are used as the inputs for the thin sheet with values applied to every cell in the model domain.

3.3 Geoelectric Field

Electric fields are induced at the surface of the Earth due to temporal variations in the magnetic field. We use the thin-sheet model of Vasseur and Weidelt (1977) to calculate these electric fields. Like Mac Manus et al. (2022) the range of valid periods have not been restricted and span from 2-minutes (corresponding to the Nyquist frequency) to the length of the geomagnetic disturbance period modeled (1440, 1866, or 2048 minutes depending on the scenario).

3.4 GIC Model

The New Zealand high-voltage AC power network consists of a large number of substations ($\sim$190) each with a varying number of transformers ($\sim$590). A number of these transformers ($\sim$55%) are Earthed and allow GIC to flow to and from ground through the transformer earthing points. The substations are connected together by $\sim$410 transmission lines of voltage ranges: 50/66 kV, 110 kV, and 220 kV.

The GIC is modeled at the transformer level following the approach of Lehtinen and Pirjola (1985) and the modification by Boteler and Pirjola (2014). This gives us the calculated current through each transformer winding and transmission line. A detailed

explanation of this process has been given in Section 2.4 of Mac Manus et al. (2022) and the references within.

To model GIC accurately in New Zealand an understanding of four key characteristics are required. These include:

- Location of Substations and their Earthed/Unearthed status.
- Transmission line connections between substation and the path these lines follow.
- Number of and type of transformers in a substations including Earthed/Unearthed status.
- Electrical resistance of all substations (via EGR), transformers, and transmission lines.

Some transformer windings in the New Zealand network are termed "upper phase" transformers. This refers to a series winding on an auto transformer between two nonzero kV buses. It is also worth noting that transformers referred to as "unearthed" are only unearthed on the high voltage side (66 kV or greater). These transformers may be earthed on the local network, at lower voltage which we are not modeling here. The local networks at lower voltages throughout New Zealand consist of higher line resistances and shorter line lengths, leading to smaller GIC and much less stress on transformers in these networks.

3.5 Spectral Scaling of GIC

Mac Manus et al. (2022) modeled the GIC during 25 disturbed periods covering weakly active periods through to large geomagnetic storms from 2001-2019. In that study they used nearly two decades of GIC observations archived by Transpower New Zealand Ltd, the national grid operator, to help validate the model output.

Validating the modeled GIC at the 73 transformers which have measured GIC across the multiple disturbance events allowed the creation of 73 unique local scaling curves. These were termed the "local multi-storm corrected power spectra" (LMSC power spectra) and provided a unique correction applied to that specific transformer to produce more accurate GIC values. By averaging all LMSC power spectra created a "nationwide multi-storm corrected power spectra" (NMSC power spectra) to improve the model at transformers without existing GIC measurements. The use of 73 LMSC power spectra provides reasonable assurance that the un-monitored transformers will be represented by those for which measurements do exist.

By scaling the model output using the observed GIC power spectra Mac Manus et al. (2022) showed that the correlations between maximum modeled and observed GIC is improved by 10-40% depending on the transformer. The Pearson Correlation Coefficients were also improved.

Since Mac Manus et al. (2022) there have been some small network resistance changes and the decommissioning of the New Plymouth substation. These changes are very minimal and result in between 0-0.5% of a change in the LMSC and NMSC power spectra. The current study makes use of the most up to date New Zealand network configuration we know of, which was provided on 26th February 2022.

4 GIC impacts on power systems

The primary GIC impact occurs at the higher voltage levels due to the long line lengths and lower line resistances. In New Zealand, ∼40% of the transmission lines are at 220 kV yet they make up 80% of the GIC flowing through transmission lines. GIC

in transformers can cause half-cycle saturation leading to a number of secondary effects. These are mentioned in Molinski (2002) and include:

- Heating of the transformer core leading to damage from the stray AC magnetic flux.
- Generation of harmonics due to deviation from the quasi sinusoidal electric current and system voltage.
- Increases in transformer magnetizing current changing the balance between the "real" power used for serving system load and "imaginary" reactive power fluctuating within the transmission system.

These effects can lead to system voltage instabilities, voltage collapse and blackouts. Real and reactive power imbalances are the most likely scenario for large transmission system impact during an extreme geomagnetic storm (NERC, 2012). The March 1989 Hydro Quebec blackout was a combination of harmonics (item 2) and power imbalances (item 3) (Bolduc, 2002; Boteler, 2019).

Transformer heating related damage has also been documented before. Examples include the New Jersey Saleem power station during March 1989 and several South African transformers as a result of the October/November 2003 geomagnetic storm (Gaunt & Coetzee, 2007). Wide-scale sudden damage of a large number of transformers due to large geomagnetic activity is unlikely. Most large-scale GIC spikes are too short in duration and should not elevate the transformer hot spot temperature to dangerous levels. However, extreme worst case scenarios are likely to have enhanced GIC with magnitudes above dangerous thresholds for extended durations . This could result in insulation damage which may cause immediate failure, or a reduction in the transformer lifetime in terms of total operational hours before a replacement is needed. A number of reports indicate how lower levels of GIC can impact the transmission system performance and efficiency by gradually degrading key system components (Forbes & St. Cyr, 2008, 2010; Gaunt, 2014).

Figure 4 is an example of the relationship between GIC and hotspot temperatures in a transformer. The hotspot heating is not instantaneous and is dependent on the GIC time series history including the amplitude and duration of GIC as well as the bulk oil and ambient temperature.

4.1 Industry GIC thresholds

The transformer related effects discussed above occur when high magnitudes of GIC flow through the transformer windings. Quantifying what is considered as high magnitude is dependent on the power network system characteristics. The Federal Energy Regulatory Commission (FERC) standard sets 75 A per phase (225 A for a three phase transformer) as the threshold for thermal impact assessment (FERC, 2015).

Transformer manufacturers use GIC capability curves to identify thermal impact thresholds. These vary based on the transformer design and need to account for high magnitude, short duration GIC and low magnitude, long duration GIC. This represents the maximum GIC the transformer would operate at without exceeding its loss of life threshold. Unfortunately details around how these curves are created and what assumptions are made are limited.

Girgis and Vedante (2013) presents the GIC capability of a transformers using loading limits recommended by the IEEE Loading Guide C57.12.91. These limits vary depending on insulation type and GIC duration but range from 140-160°C for 30-minute durations and 160-180°C for 2-minute GIC pulses. These limits are set to reduce the rate of degradation of the insulation used in the transformer and to prevent the buildup of gas bubbles in the oil. For 30 minutes a GIC of 150 A/phase (600 A/phase) is required

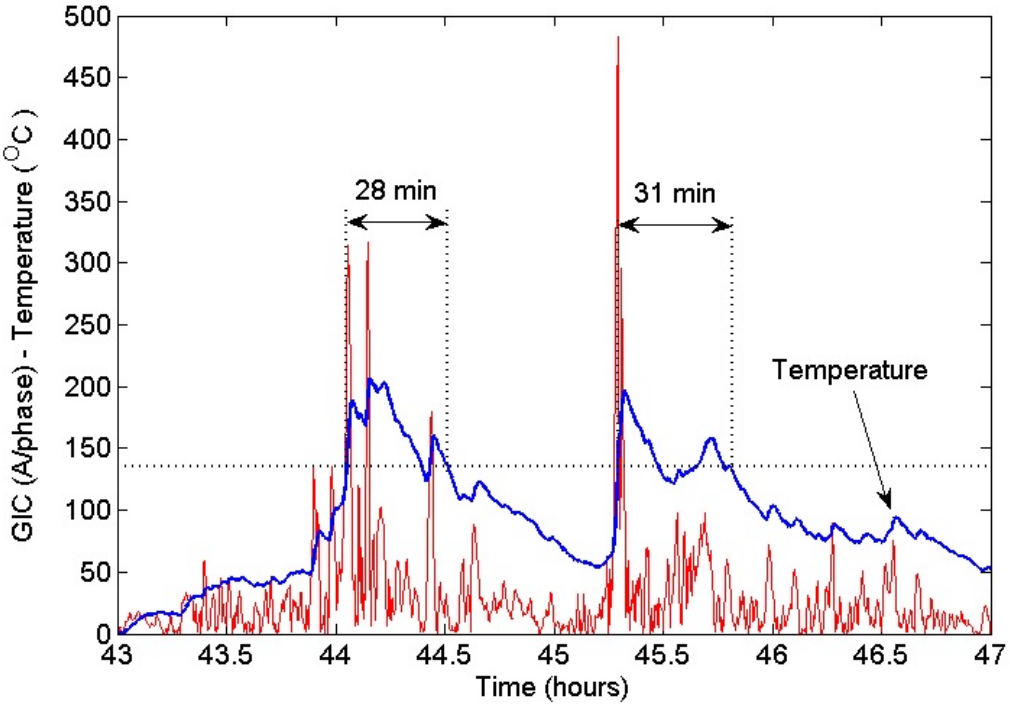

Figure 4: Example showing GIC/temperature relationship. The Blue line indicates temperature and the red is the magnitude of GIC/phase. From Marti et al. (2013).

to reach 140°C (160°C) while for short 2-minute GIC pulses, values of 520A/phase (900 A/phase) are required to reach 160°C (180°C).

4.2 Transpower danger threshold levels

Transpower New Zealand Ltd have provided the authors of this study with current thresholds and durations that would minimise either:

- excessive loss of transformer life (>20% of transformer life) or
- the probability of catastrophic failure either through insulating oil thermal breakdown and hydrogen bubble formation or overheating of conductors or their insulation structure degrading.

The threshold and duration values were determined by considered the transformer susceptibility and site specific GIC currents as outlined in the IEEE C57.163-2015 guide while allowing for the substantially greater magnitude and duration of base and peak GIC currents observed and modeled in New Zealand. These values were correlated with the expected effect on a new 220/110 kV three phase three limb core transformer design completed by one of Transpower's transformer suppliers. The design looked at winding and core structure hot spot temperatures and reported the various current time and duration combinations required to cause either excessive life of the transformer to be lost or for the transformer to enter a state where the probability of catastrophic insulation failure was very high. The tests and modeling were performed for a modern three phase three limb unit while reductions of a factor 10 have been applied to single phase units. Table 1 shows the current and duration thresholds from this test corresponding to an oil temperature of 180°C.

Table 1: Tolerable duration of mean absolute current vs cumulative time for three phase three limb and single phase transformer. This corresponds to the thresholds required to reach 180°C

Danger Level	1	2	3	4	5
3phase					
-cumulative time [minutes]	240	180	120	30	15
-mean current [$\|A\|$]	200	300	500	750	1000
1phase					
-cumulative time [minutes]	240	180	120	30	15
-mean current [$\|A\|$]	20	30	50	75	100

Note that "Danger Level" 1 is not inherently better than danger level 5. All of the danger levels in Table 1 are a set of industry provided GIC levels to avoid because they should all elevate the transformer oil temperature to 180°C , despite spanning a range of mean currents and time periods. However, in the following descriptions of the modeling results we consider danger level 1 as the least concerning, and danger level 5 as the most concerning, primarily due to the higher GIC levels requiring more rapid response times in order to stop the transformer reaching the critical temperature threshold.

5 Extreme storm results

GIC output for the nine extreme storm scenarios discussed in section 2 have been calculated for all the earthed transformers in the New Zealand power network. In each case, every transformer with GIC has been checked to see if it exceeds the magnitude and time thresholds given in Table 1 for each danger level, taking into account of whether the transformers is of 3-phase 3-limb design or single phase.

We will initially discuss the three scenarios based of the March 1989 event.

5.1 March 1989 scenarios

Figure 5 shows the time series of the modeled GIC for "LVR HWB T6". In this Figure a comparison between the original GIC (blue) and the NMSC corrected GIC (green) is given. Here, we find a maximum GIC of 2600 A (up from 2200 A for the original GIC calculation) leading to a 60-minute mean of 720 A. This is the GIC flowing through the 0-110 kV node of the #6 transformer at the Halfway Bush (HWB) substation in Dunedin. HWB T6 is an autotransformer, hence it also has GIC flowing through the 110-220 kV node (HVR HWB T6). Throughout the rest of the paper, unless otherwise mentioned the GIC values presented are the NMSC corrected values. The colored bars at the bottom of the figure represent time periods for which the corresponding danger level was reached (Cyan (1), Yellow (2), Orange (3), Red (4), Maroon (5)). Each instance in time for which a danger level is reached indicates the mean current over the previous "X" amount of minutes for said danger level was above the required threshold. For example, in Figure 5, danger level 1 is first reached at 08:03 UT. This requires the mean absolute GIC in the previous four hours (4:03 - 8:03 UT) to exceed 200 A.

The locations that meet the Transpower danger thresholds are given in the map in Figure 6. The three panels represent the three different latitude scaling methods. Each colored shape represents a substations that contains at least one transformer that meets

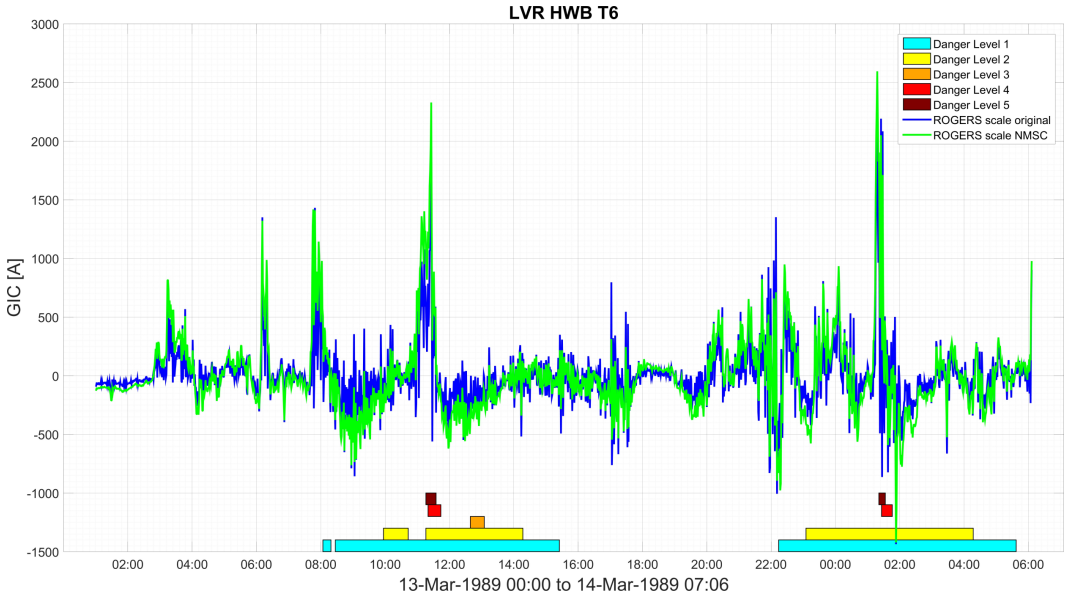

Figure 5: Modeled GIC for HWB T6 during the March 1989 ROGERS latitude scenario. In green is the output after the NMSC correction. In blue is the original modeled GIC for comparison. The colored bars at the bottom represent time periods for which the corresponding danger level was reached (Cyan (1), Yellow (2), Orange (3), Red (4), Maroon (5))

at the specific danger level (Cyan square (1), Yellow diamond (2), Orange triangle (3), Red hexagon (4), Maroon star (5)).

For the ROGERS latitude variation 44 transformers (13% of the total earthed transformers) reach at least danger level 1, shown by the colored shapes in the left hand panel of Figure 6. Of these 38 (those given by the maroon stars in the left hand panel) reach the highest danger level. This indicates all of those 38 have GIC which exceed 1000 A mean (or 100 A for single phase) over a 15 minute period. For this scenario the largest mean GIC are recorded at SDN T2 (South Dunedin) and HWB T6 with a mean absolute current over 15 minutes of 2250 and 1530 A respectively. The South Dunedin and Halfway Bush substations are within 5km of each other and are located in the city of Dunedin in the lower South Island. They have consistently been the two transformers with the largest observed GIC during past geomagnetic events. The left hand panel of Figure 6 shows that the majority of the transformers identified are located in the lower South Island. However, a few locations in the North Island also reach the highest danger level. These include the substations of Stratford (SFD) on the North Island west coast, Redclyffe (RDF) on the east coast, and Henderson (HEN) in the city of Auckland. All these transformers exceeding the threshold are single phase transformers that until the end of 2021, had no GIC measurements. Rodger et al. (2020) showed a correlation between even-order harmonics and large GIC at sites with measured GIC at the instrumented substations in the South Island and also showed the presence of harmonics at the three North Island substations mentioned, supporting the validity of the modeling output showing increased GIC activity at these locations. Since 2021, LEMs to measure GIC have been installed at multiple new locations in the North Island such as HEN and Bunnythorpe (BPE).

Using the NERC latitude variation produces similar results for this scaled time variation. Here a larger number (53, 16% of total) exceed a danger level threshold, however

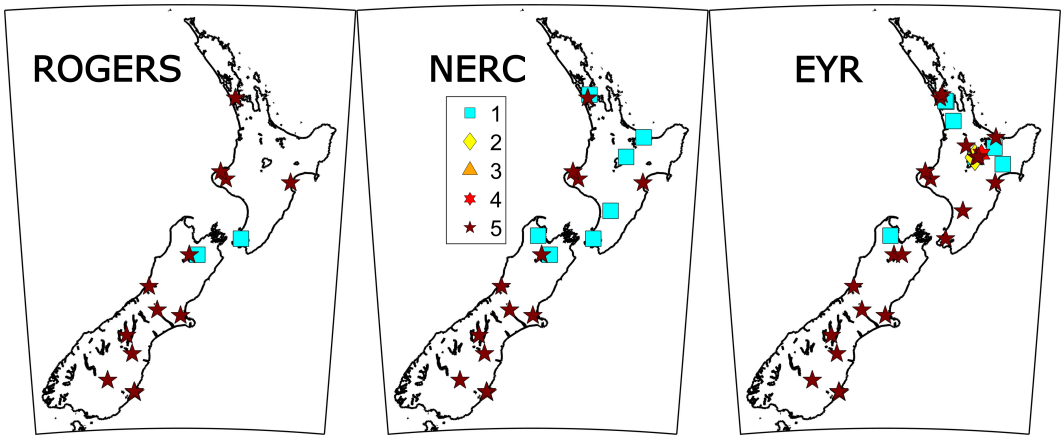

Figure 6: Substations that meet the various Transpower danger levels for the ROGERS, NERC, and constant Eyrewell (EYR) geomagnetic latitude variations for the March 1989 extreme storm scenario. The colored shapes represent the maximum danger level that a transformer at the given substation reached.

the same transformers reach the largest threshold (shown by the same maroon stars in the left and center panel of Figure 6). This indicates consistency in which transformers have the largest modeled GIC. Some additional locations reach the lower threshold mean of 200/20 A (three or single phase) for a duration of four hours. These locations are primarily in the center of the North island (shown by the additional cyan squares in the middle panel). This is understandable when looking at the magnetic field in Figures 2 and 3. The larger H' in the central North Island for the NERC latitude variation leads to larger electric fields and therefore larger GIC.

The right hand panel of Figure 6 shows the situation for a non-spatially varying magnetic field. This produces larger magnetic and electric field in the North Island as shown by the increased number of substations reaching the various danger levels. In total 81 (24%) of transformers exceed a danger level threshold. While the non-varying field is not particularly physically valid, it provides a different form of extreme test, and provides additional information on the transformers which might be at risk (and likely more importantly, those unlikely to be at risk).

Table 2 lists the top 10 transformers for each latitude variation approach by mean GIC over a 60-minute interval. The maximum GIC during the event is also given in the last column. This table is independent of transformer type as there is no GIC threshold requirement. The table demonstrates that the same transformers typically have the largest GIC regardless of latitude variation as eight of the top 10 occur for both the ROGERS and NERC scenarios (six are also present for the constant scenario). When considering all transformers we find that 58(18% of total), 69(21%) and 95(29%) transformers exceed 100 A for a 60-minute mean GIC for the three latitude variation scenarios, respectively.

5.2 October 2003 scenarios

The results for the October 2003 ROGERS latitude variation are very similar to those from the equivalent March 1989 scenario. By looking at the left hand panel of Figure 6 and 7 we can see that typically the same locations reach the Transpower danger levels. In fact, the exact same 44 transformers reach the danger levels. In contrast 28 transformers reach the highest danger level (i.e., level 5), down from 38 for the March

1989 event. This indicates smaller mean currents occurring within the 15 minute interval required to exceed the threshold and can be seen by the larger number of non-maroon colored shapes in the left hand panel of Figure 7 when compared to the left hand panel of Figure 6.

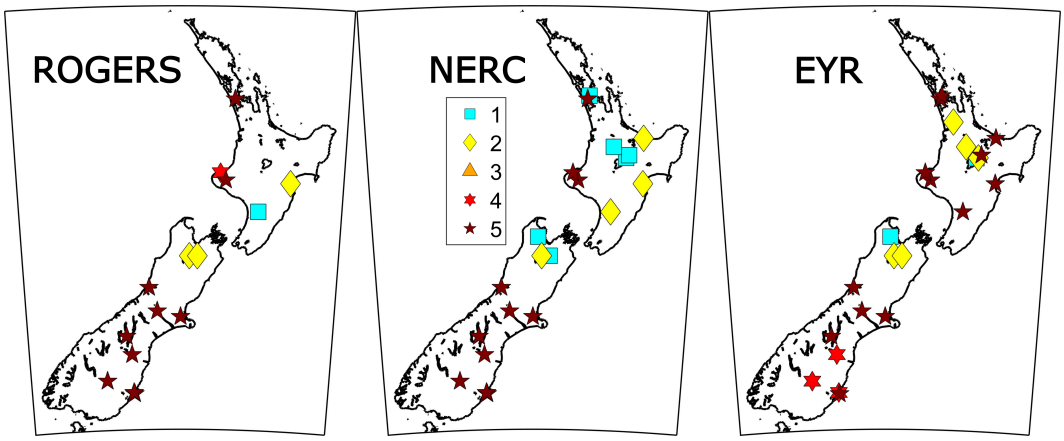

Figure 7: Substations that meet the various Transpower danger levels for the ROGERS, NERC, and constant Eyrewell (EYR) geomagnetic latitude variations for the October 2003 extreme storm scenario. The colored shapes represent the maximum danger level that a transformer at the given substation reached.

Likewise, for the NERC latitude variation the results are very similar. A total of 54 (up one from 53) transformers exceed a danger level threshold. For the constant Eyrewell condition the results differ the most from the earlier scenario. Here 67 (20%) reached a danger level threshold. This is down from 81 transformers for the March 1989 scenario. However the biggest difference comes when we look at the danger level that each transformer reached. We find a number of transformers that reached the lower danger level (Cyan square) for March 1989 increasing to the second danger level (Yellow diamond) for October 2003. We also see the Halfway Bush substation does not reach the largest danger threshold in this case. This is the only occurrence of this in the nine extreme storm scenarios.

Table 3 shows the mean GIC over a 60-minute interval as well as the maximum GIC during the storm event. We again see similarities with Table 2 in that eight out of 10 transformers occur in the top 10 for both the March 1989 and October 2003 ROGERS latitude scenarios. Likewise eight out of 10 occur for both events with the NERC latitude variation and eight out of 10 for the constant Eyrewell latitude variation. This shows the consistency in which transformers have the largest GIC across multiple extreme storm scenarios. Looking at all transformers we find that 49(15%), 58(18%) and 77(23%) transformers exceed 100 A, 60-minute mean GIC. This is down by 9-18 (3-6%) transformers when compared with the March 1989 scenarios.

5.3 September 2017 scenarios

The three scenarios for the extreme storm based on the magnetic field time series from September 2017 produce the largest GIC of all scenarios modeled. We can see this visually in Figure 8. More transformers reach the various danger levels when compared to the corresponding latitude variations for either the March 1989 and October 2003 extreme storm scenarios. Across the three latitude variations scenarios 66 (20%), 91 (27%), and 115 (35%) transformers reach a danger level threshold.

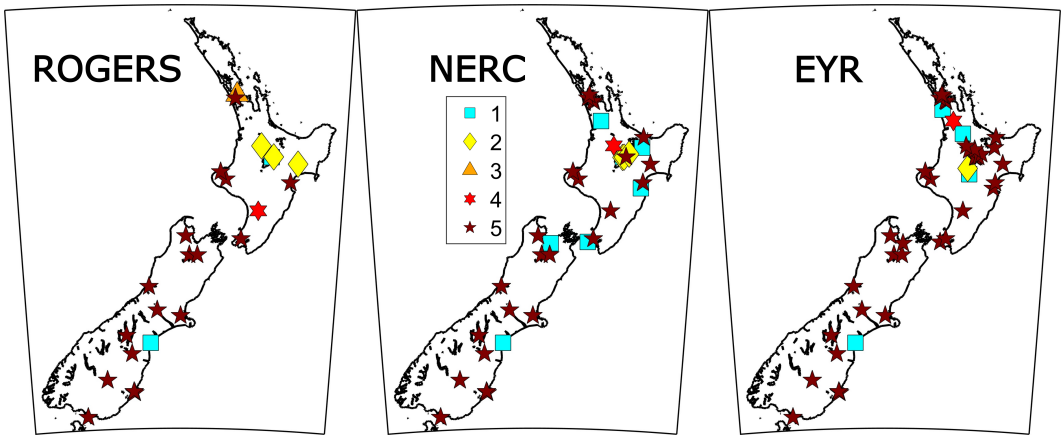

Figure 8: Substations that meet the various Transpower danger levels for the ROGERS, NERC, and constant Eyrewell (EYR) geomagnetic latitude variations for the September 2017 extreme storm scenario. The colored shapes represent the maximum danger level that a transformer at the given substation reached.

One can also clearly see larger mean and maximum currents in Table 4 when compared to Tables 2 and 3. A significantly larger number of transformers have a mean 60-minute GIC above 100 A. This is 118 (36%), 138 (42%), and 182 (55%) for the ROGERS, NERC and constant EYR latitude variations. The likely cause for such large GIC associated with the three September 2017 scenarios is due to the *H'* value of 40 nT/min associated with the reference magnetic field. This is a rather small *H'* corresponding with the large GIC measurements (max of 49 A) in New Zealand during that event (Mac Manus et al., 2022). This highlights that the magnetic field waveform used for the extreme storm scenarios based of September 2017 represent the worst case scenarios.

5.4 Overall findings

Figure 9 shows the mean 60-minute GIC at every earthed transformer. Each panel shows one of the extreme storm scenarios modeled. This provides a visual representation of Tables 2, 3, and 4 extended to include all 331 earthed transformers that will experience some level of GIC. The order is sorted based on the order of the largest GIC calculated for the October 2003 ROGERS latitude variation scenario and kept consistent amongst all scenarios. Here we can see the increased GIC for the September 2017 scenarios and constant Eyrewell (no latitude variation) scenarios (e.g the bottom row and last column for all scenarios).

This figure also illustrates that the same transformers occur near the top of all scenarios, i.e., the "hot spot" transformers with the largest GIC are essentially the same across all scenarios, despite the strong differences between these scenarios. Table 5 supports this finding and shows the mean ranking for the top 30 transformers along with their ranking for each individual scenario. The substation locations of these 30 transformers are shown in Figure 10 along with the location of the Eyrewell magnetic observatory (given by the blue star). The AC transmission network is shown by the blue lines. We suggest that these are the transformers which should be focused upon when considering the economic disruption caused by extreme space weather, and any possible mitigation approaches. Note this map extends across both the North and South Islands, including most (but not all) major population centers.

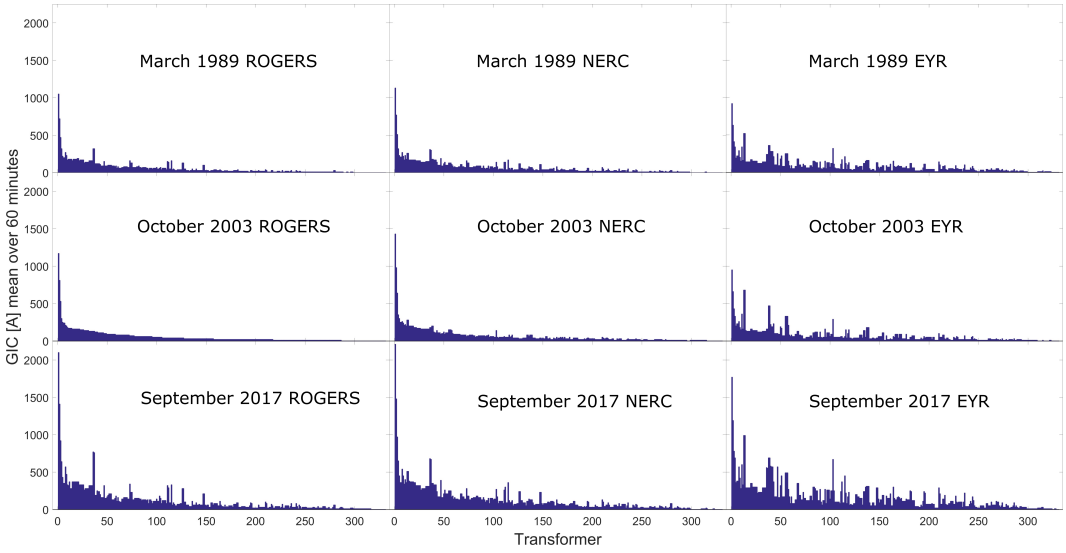

Figure 9: Mean 60-minute GIC at each transformer for the nine extreme storm scenarios modeled.

One of the transformers shown in Figure 10 is at the South Dunedin substation (HVR SDN T2). As Table 5 shows, this transformer consistently has the largest 60-minute mean GIC for every extreme scenario modeled. In the supplementary material, Figures S1-S9 show the GIC time series for this transformer for each scenario (similar to Figure 5). The colored bars at the bottom of the figure represent time periods for which the corresponding danger level was reached (Cyan (1), Yellow (2), Orange (3), Red (4), Maroon (5)). This highlights that a danger level is often reached for multiple continuous minutes throughout the extreme storm scenario, further increasing the likelihood of transformer failure and network disruption.

Tables 2, 3, and 4 provide some insights into the variability of the different extreme storm scenarios. The mean 60-minute GIC for the top 10 transformers in the March 1989 scenarios is very similar if not slightly smaller than the October 2003 scenarios while in contrast the maximum GIC is approximately double. The September 2017 scenarios are large for both the mean and max GIC. Multiple different extreme storm scenarios are required to give a better understanding of the expected instantaneous max GIC and long term mean GIC.

6 Summary and Discussion

Extreme geomagnetic storms can lead to large GIC in earthed transformer windings that have the potential to damage the transformer and disrupt the power supply. Not only is the concern from short lived GIC pulses, but also from elevated GIC that last for extended periods of time. Such elevated GIC over significant time can cause transformer core temperature increases that can reduce the transformers life span; in extreme cases this may cause a transformer to be physically damaged during the storm itself.

The results presented in this study are all relative to the selected reference maximum *H'* of 4000 nT/min used at the location of the Eyrewell magnetometer. A larger value such as 6000 nT/min given in Thomson et al. (2011) corresponding to the upper limit of the 95% confidence interval for a 200 year return event could have been selected, as this would also be "reasonable" for an extreme geomagnetic storm impacting New Zealand.

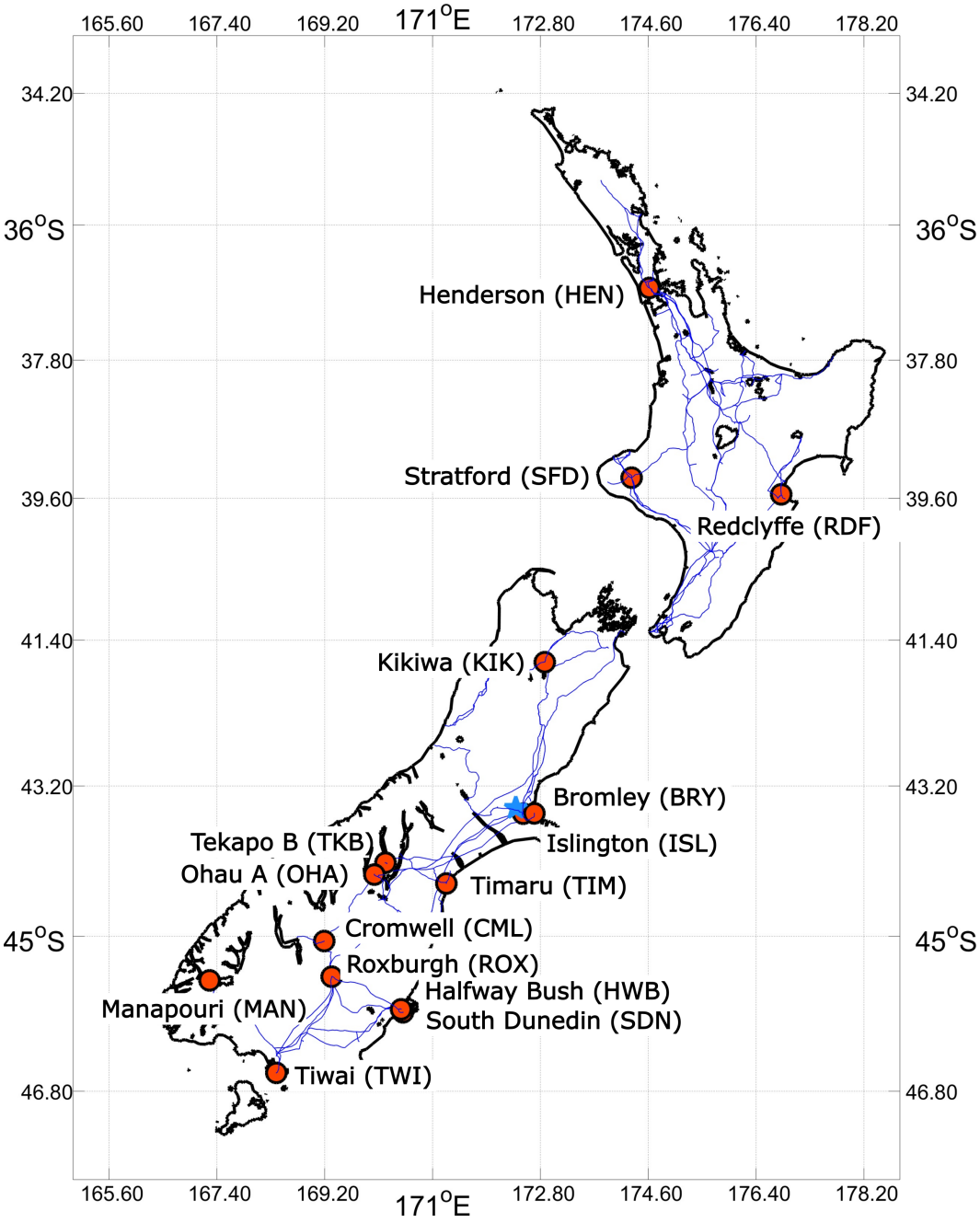

Figure 10: Location of the top 30 transformers (given in Table 5) ranked by mean GIC over a 60-minute duration. These are given by the orange circles while the Eyrewell magnetic observatory is shown as a blue star.

Given the range of maximum rates of change for UK-extreme storms discussed earlier, the 4000 nT/min value we use also appears "reasonable" for a geomagnetically mid-latitude country, like New Zealand. A higher *H'* level of 6000 nT/min would result in 16-47% of transformers reaching a danger level thresholds (compared with 13-35% for 4000 nT/min) and an increase in the mean and maximum GIC throughout all transformers in the network. This emphasises the importance of the choice of the maximum *H'* used in the scenarios, as a larger value will push more transformers onto the risk list.

Table 5 shows that the 60-minute mean GIC is consistently largest for a transformer at the South Dunedin substation (HVR SDN T2). This is located in the city of Dunedin in the South Island while the largest GIC in the North Island is at the Henderson substation (LVR HEN T1) in the city of Auckland. The maximum geoelectric field in the region for which transmission lines flow into the South Dunedin substation is between 11-16 V/km depending on the extreme storm scenario while for Henderson this value varies between 6-9 V/km. These values appear approximately consistent with the range of peak electric fields presented in the literature for extreme events. Kappenman (2004) suggests a 100 year return level event electric field of approximately 20 V/km while a worst case Carrington event could be larger. For a similar geomagnetic latitude country like the UK, Beggan et al. (2013) reports an expected electric field of 10 V/km for extreme storms. The NERC guidelines for GIC mitigation given in U.S., TPL-007-1 use a maximum electric field magnitude of 8 V/km for a 100 year return level event. Similarly, Winter et al. (2017) used spectral scaling techniques to estimate peak electric field of 9 V/km that may be associated with a geomagnetic event of similar magnitude to the Carrington event but noted that the uncertainty may be between 4-20 V/km.

Our goal in this study has been to provide reasonable assurance of the magnitude and duration of large GIC at multiple transformers during an extreme storm. To do this we looked at nine unique representations of a worst case extreme geomagnetic storm representing various magnetic field waveforms scaled to an extreme storm threshold and having different latitude variations. A peak mean absolute GIC over a 60-minute window of 920-2210 A and an instantaneous one-minute time resolution maximum GIC of 1590-4920 A is expected for a worst case extreme storm scenario. We find there is a strong consistency in the Earthed transformers which reach the industry-provided "danger levels". When we use three different large geomagnetic storms to produce the time variation for our extreme storms, we find there is only a small difference between the at risk transformers, i.e., the hot spots are largely independent of the selected time-variation. There is a more significant variation in the at risk transformer list depending on the latitude variation selected for the extreme storm modeling; however we note the more realistic scenarios (for which there is some latitude variation) are very similar, while the large difference comes from the less realistic representation of a constant field change with latitude. This finding is highly useful, as it suggests we can take the transformers identified as hotspots and focus mitigation approaches on that equipment. We find that between 13 and 35% of all Earthed transformers would reach a danger level provided by Transpower. This corresponds to between 44 and 115 transformers throughout New Zealand which may need to be replaced costing many millions and taking years to complete. Clearly, these are the locations were mitigation and protection systems should be considered in the future.

Ongoing work with Transpower is currently underway to develop effective and realistic mitigation strategies that can be implemented if an extreme storm is predicted. The aim will be to reduce the disruption and damage to the New Zealand power network. We intend to report on those approaches in a future study.

Data Availability

The New Zealand electrical transmission network's DC characteristics and DC measurements were provided to us by Transpower New Zealand with caveats and restrictions. This includes requirements of permission before all publications and presentations and no ability to provide the observations themselves. In addition, we are unable to provide the New Zealand network characteristics due to commercial sensitivity. Requests for access to these characteristics and the DC measurements need to be made to Transpower New Zealand. At this time the contact point is Michael Dalzell (Michael.Dalzell@transpower.co.nz).

Acknowledgments

This research was supported by the New Zealand Ministry of Business, Innovation and Employment Endeavour Fund Research Programme contract UOOX2002. The authors would like to thank Transpower New Zealand for supporting this study. The results presented in this paper rely on the data collected at Eyrewell. We thank the Institute of Geological and Nuclear Sciences Limited (GNS), for supporting its operation and INTERMAGNET for promoting high standards of magnetic observatory practice (www.intermagnet.org).

References

Ahn, B. H., Chen, G. X., Sun, W., Gjerloev, J. W., Kamide, Y., Sigwarth, J. B., & Frank, L. A. (2005). Equatorward expansion of the westward electrojet during magnetically disturbed periods. *Journal of Geophysical Research: Space Physics*, *110*(A1), 1–11. doi: 10.1029/2004JA010553

Beggan, C. D., Beamish, D., Richards, A., Kelly, G. S., & Alan, A. W. (2013). Prediction of extreme geomagnetically induced currents in the UK high-voltage network. *Space Weather*, *11*(7), 407–419. doi: 10.1002/swe.20065

Bolduc, L. (2002). GIC observations and studies in the Hydro-Québec power system. *Journal of Atmospheric and Solar-Terrestrial Physics*, *64*(16), 1793–1802. doi: 10.1016/S1364-6826(02)00128-1

Boteler, D. H. (2019). A 21st Century View of the March 1989 Magnetic Storm. *Space Weather*, *17*(10), 1427–1441. doi: 10.1029/2019SW002278

Boteler, D. H., & Pirjola, R. J. (2014, sep). Comparison of methods for modelling geomagnetically induced currents. *Annales Geophysicae*, *32*(9), 1177–1187. Retrieved from `http://www.ann-geophys.net/32/1177/2014/` doi: 10.5194/angeo-32-1177-2014

Cagniard, L. (1953). Basic Theory of the Magneto-Telluric Method of Geophysical Prospecting. *Geophysics*, *18*(3), 605–635. doi: 10.1190/1.1437915

Cannon, P. (2013). *Extreme space weather: impacts on engineered systems and infrastructures.* Retrieved from `http://www.raeng.org.uk/news/publications/list/reports/Space{\_}Weather{\_}Full{\_}Report{\_}Final.PDF`

Chapman, S. C., Horne, R. B., & Watkins, N. W. (2020). Using the aa Index Over the Last 14 Solar Cycles to Characterize Extreme Geomagnetic Activity. *Geophysical Research Letters*, *47*(3). doi: 10.1029/2019GL086524

Clilverd, M. A., Rodger, C. J., Brundell, J. B., Dalzell, M., Martin, I., Mac Manus, D. H., ... Obana, Y. (2018). Long-Lasting Geomagnetically Induced Currents and Harmonic Distortion Observed in New Zealand During the 7–8 September 2017 Disturbed Period. *Space Weather*, *16*(6), 704–717. doi: 10.1029/2018SW001822

Clilverd, M. A., Rodger, C. J., Freeman, M. P., Brundell, J. B., Manus, D. H. M., Dalzell, M., ... Frame, I. (2021). Geomagnetically induced currents during the 07 – 08 September 2017 disturbed period : a global perspective. *Space Weather Space Climate*.

Divett, T., Ingham, M., Beggan, C. D., Richardson, G. S., Rodger, C. J., Thom-

son, A. W., & Dalzell, M. (2017). Modeling Geoelectric Fields and Geomagnetically Induced Currents Around New Zealand to Explore GIC in the South Island's Electrical Transmission Network. *Space Weather*, *15*(10). doi: 10.1002/2017SW001697

Divett, T., Mac Manus, D. H., Richardson, G. S., Beggan, C. D., Rodger, C. J., Ingham, M., ... Obana, Y. (2020). Geomagnetically Induced Current Model Validation From New Zealand's South Island. *Space Weather*, *18*(8). doi: 10.1029/2020SW002494

Divett, T., Richardson, G. S., Beggan, C. D., Rodger, C. J., Boteler, D. H., Ingham, M., ... Dalzell, M. (2018). Transformer-Level Modeling of Geomagnetically Induced Currents in New Zealand's South Island. *Space Weather*, *16*(6). doi: 10.1029/2018SW001814

FERC. (2015). Reliability standard for transmission system planned performance for geomagnetic distur- bance events. *Federal Energy Regulatory Commission*, *80*(100), 18 CFR Part 40, Docket No. RM15–11–000.

Forbes, K. F., & St. Cyr, O. C. (2008). Solar activity and economic fundamentals: Evidence from 12 geographically disparate power grids. *Space Weather*, *6*(10), 1–20. doi: 10.1029/2007SW000350

Forbes, K. F., & St. Cyr, O. C. (2010). An anatomy of space weather's electricity market impact: Case of the PJM power grid and the performance of its 500 kV transformers. *Space Weather*, *8*(9), 1–24. doi: 10.1029/2009SW000498

Gaunt, C. T. (2014). Reducing uncertainty - Responses for electricity utilities to severe solar storms. *Journal of Space Weather and Space Climate*, *4*, 1–7. doi: 10.1051/swsc/2013058

Gaunt, C. T., & Coetzee, G. (2007). Transformer failures in regions incorrectly considered to have low GIC-risk. *2007 IEEE Lausanne POWERTECH, Proceedings*, 807–812. doi: 10.1109/PCT.2007.4538419

Girgis, R., & Vedante, K. (2013). Methodology for evaluating the impact of GIC and GIC capability of power transformer designs. *IEEE Power and Energy Society General Meeting*, 1–5. doi: 10.1109/PESMG.2013.6672911

Gombosi, T. I. (1998). *Physics of the Space Environment*. Cambridge University Press.

Hapgood, M., Angling, M., Attrill, G., Bisi, M., Burnett, C., Cannon, P., ... Willis, M. (2020). Summary of space weather worst-case environments (2nd revised edition) - RAL-TR-2020-005. *UKRI - RAL Technical Report*, 56. Retrieved from `https://epubs.stfc.ac.uk/manifestation/46642578/RAL-TR-2020-005.pdf`

Huttunen, K. E., Kilpua, S. P., Pulkkinen, A., Viljanen, A., & Tanskanen, E. (2008). Solar wind drivers of large geomagnetically induced currents during the solar cycle 23. *Space Weather*, *6*(10), 1–8. doi: 10.1029/2007SW000374

Ingham, M., Rodger, C. J., Divett, T., Dalzell, M., & Petersen, T. (2017). Assessment of GIC Based On Transfer Function Analysis. *Space Weather*, *15*(12), 1615–1627. doi: 10.1002/2017SW001707

Kappenman, J. G. (2004). The Evolving Vulnerability of Electric Power Grids. *Space Weather*, *2*(1), n/a–n/a. doi: 10.1029/2003sw000028

Kappenman, J. G. (2006). Great geomagnetic storms and extreme impulsive geomagnetic field disturbance events - An analysis of observational evidence including the great storm of May 1921. *Advances in Space Research*, *38*(2), 188–199. doi: 10.1016/j.asr.2005.08.055

Kappenman, J. G., & Albertson, D. (1990). *Bracing for the geomagnetic storms* (Vol. 27) (No. 3). doi: 10.1109/6.48847

Kivelson, M. G., & Russell, C. T. (1995). *Introduction to Space Physics*. Cambridge University press.

Lehtinen, M., & Pirjola, R. (1985). Currents produced in earthed conductor networks by geomagnetically-induced electric fields. *Annales Geophysicae*.

Lloyd. (2013). *Solar Storm Risk to the North American Electric Grid* (Tech. Rep.).

Love, J. J. (2012). Credible occurrence probabilities for extreme geophysical events: Earthquakes, volcanic eruptions, magnetic storms. *Geophysical Research Letters*, *39*(10), 1–6. doi: 10.1029/2012GL051431

Love, J. J., Coïsson, P., & Pulkkinen, A. (2016). Global statistical maps of extreme-event magnetic observatory 1 min first differences in horizontal intensity. *Geophysical Research Letters*, 4126–4135. doi: 10.1002/2016GL068664.Analysis

Mac Manus, D. H., Rodger, C. J., Dalzell, M., Thomson, A. W., Clilverd, M. A., Petersen, T., ... Divett, T. (2017). Long-term geomagnetically induced current observations in New Zealand: Earth return corrections and geomagnetic field driver. *Space Weather*, *15*(8), 1020–1038. doi: 10.1002/2017SW001635

Mac Manus, D. H., Rodger, C. J., Ingham, M., Clilverd, M. A., Dalzell, M., Divett, T., ... Petersen, T. (2022). Geomagnetically Induced Current Model in New Zealand Across Multiple Disturbances: Validation and Extension to Non-Monitored Transformers. *Space Weather*, *20*(2). doi: 10.1029/2021sw002955

Marti, L., Rezaei-Zare, A., & Narang, A. (2013). Simulation of transformer hotspot heating due to geomagnetically induced currents. *IEEE Transactions on Power Delivery*, *28*(1), 320–327. doi: 10.1109/TPWRD.2012.2224674

Molinski, T. S. (2002). Why utilities respect geomagnetically induced currents. *Journal of Atmospheric and Solar-Terrestrial Physics*, *64*(16), 1765–1778. doi: 10.1016/S1364-6826(02)00126-8

Mukhtar, K., Ingham, M., Rodger, C. J., Mac Manus, D. H., Divett, T., Heise, W., ... Petersen, T. (2020). Calculation of GIC in the North Island of New Zealand Using MT Data and Thin-Sheet Modeling. *Space Weather*, *18*(11). doi: 10.1029/2020SW002580

National Research Council. (2008). *Severe Space Weather Events–Understanding Societal and Economic Impacts*. doi: 10.17226/12507

NERC. (2012). Effects of Geomagnetic Disturbances on the Bulk Power System. *North American Electric Reliability Corporation*.

NERC. (2016). Benchmark Geomagnetic Disturbance Event Description. *North American Electric Reliability Corporation*.

Ngwira, C. M., Pulkkinen, A., Wilder, F. D., & Crowley, G. (2013). Extended study of extreme geoelectric field event scenarios for geomagnetically induced current applications. *Space Weather*, *11*(3), 121–131. doi: 10.1002/swe.20021

Ohtani, S., Fujii, R., Hesse, M., & Lysak, R. (2000). *Magnetospheric Current Systems*. AGU Geophys. Monogr. 118, AGU, Washington, D. C.

Oughton, E. J., Skelton, A., Horne, R. B., Thomson, A. W., & Gaunt, C. T. (2017). Quantifying the daily economic impact of extreme space weather due to failure in electricity transmission infrastructure. *Space Weather*, *15*(1), 65–83. doi: 10.1002/2016SW001491

Pulkkinen, A., Bernabeu, E., Eichner, J., Beggan, C., & Thomson, A. W. (2012). Generation of 100-year geomagnetically induced current scenarios. *Space Weather*, *10*(4), 1–19. doi: 10.1029/2011SW000750

Pulkkinen, A., Lindahl, S., Viljanen, A., & Pirjola, R. (2005). Geomagnetic storm of 29-31 October 2003: Geomagnetically induced currents and their relation to problems in the Swedish high-voltage power transmission system. *Space Weather*, *3*(8). doi: 10.1029/2004SW000123

Riley, P. (2012). On the probability of occurrence of extreme space weather events. *Space Weather*, *10*(2), 1–12. doi: 10.1029/2011SW000734

Riley, P., & Love, J. J. (2017). Extreme geomagnetic storms: Probabilistic forecasts and their uncertainties. *Space Weather*, *15*(1), 53–64. doi: 10.1002/2016SW001470

Rodger, C. J., Clilverd, M. A., Mac Manus, D. H., Martin, I., Dalzell, M., Brundell, J. B., ... Watson, N. R. (2020). Geomagnetically Induced Currents and Harmonic Distortion: Storm-Time Observations From New Zealand. *Space*

Weather, *18*(3), 1–20. doi: 10.1029/2019SW002387

Rogers, N. C., Wild, J. A., Eastoe, E. F., Gjerloev, J. W., & Thomson, A. W. (2020). A global climatological model of extreme geomagnetic field fluctuations. *Journal of Space Weather and Space Climate*, *10*, 1–19. doi: 10.1051/swsc/2020008

Thomson, A. W., Dawson, E. B., & Reay, S. J. (2011). Quantifying extreme behavior in geomagnetic activity. *Space Weather*, *9*(10), 1–12. doi: 10.1029/2011SW000696

Vasseur, G., & Weidelt, P. (1977). Bimodal electromagnetic induction in non-uniform thin sheets with an application to the northern Pyrenean induction anomaly. *Geophysical Journal of the Royal Astronomical Society*, *51*(3), 669–690. doi: 10.1111/j.1365-246X.1977.tb04213.x

Viljanen, A., Nevanlinna, H., Pajunpää, K., & Pulkkinen, A. (2001, sep). Time derivative of the horizontal geomagnetic field as an activity indicator. *Annales Geophysicae*, *19*(9), 1107–1118. Retrieved from `https://angeo.copernicus.org/articles/19/1107/2001/` doi: 10.5194/angeo-19-1107-2001

Weigel, R. S., & Baker, D. N. (2003). Probability distribution invariance of 1-minute auroral-zone geomagnetic field fluctuations. *Geophysical Research Letters*, *30*(23), 1–4. doi: 10.1029/2003GL018470

Winter, L. M., Gannon, J., Pernak, R., Huston, S., Quinn, R., Pope, E., ... Crocker, N. (2017). Spectral scaling technique to determine extreme Carrington-level geomagnetically induced currents effects. *Space Weather*, *15*(5), 713–725. doi: 10.1002/2016SW001586

Table 2: Top 10 transformers with the largest mean absolute GIC over a 60-minute interval during the three March 1989 extreme storm scenarios. The instantaneous one-minute time resolution maximum GIC is also given for those transformers.

Extreme storm based on March 1989		
ROGERS latitude variation		
Transformer	GIC [A](mean)	GIC [A](max)
HVR SDN T2	1050	3750
LVR HWB T6	720	2600
HVR HWB T6	470	1720
HVR TWI T1	320	1120
HVR TWI T2	320	1110
LVR ISL T6	320	1080
HVR KIK T2	270	900
HVR TIM T5	230	770
HVR HWB T3	220	790
HVR BRY T7	200	780
NERC latitude variation		
Transformer	GIC [A](mean)	GIC [A](max)
HVR SDN T2	1130	3780
LVR HWB T6	770	2610
HVR HWB T6	510	1730
LVR ISL T6	320	1120
HVR TWI T1	310	1150
HVR TWI T2	300	1140
HVR KIK T2	270	920
LVR HEN T1	260	890
LVR HEN T5	260	890
HVR HWB T3	230	800
Constant EYR magnetic field		
Transformer	GIC [A](mean)	GIC [A](max)
HVR SDN T2	920	3040
LVR HWB T6	630	2100
LVR HEN T1	520	1910
LVR HEN T5	520	1910
HVR HWB T6	410	1380
HVR HEN T1	360	1320
HVR HEN T5	360	1320
LVR ISL T6	340	1140
HVR SFD T10	340	1110
HVR WRD T7	320	990

Table 3: Top 10 transformers with the largest mean absolute GIC over a 60-minute interval during the three October 2003 extreme storm scenarios. The instantaneous one-minute time resolution maximum GIC is also given for those transformers.

Extreme storm based on October 2003

ROGERS latitude variation		
Transformer	GIC [A](mean)	GIC [A](max)
HVR SDN T2	1170	1890
LVR HWB T6	810	1320
HVR HWB T6	530	870
LVR ISL T6	300	540
HVR HWB T3	250	400
HVR BRY T7	240	440
HVR BRY T5	240	440
HVR KIK T2	210	380
HVR TIM T5	200	350
LVR CML T8	180	320
NERC latitude variation		
Transformer	GIC [A](mean)	GIC [A](max)
HVR SDN T2	1430	2190
LVR HWB T6	980	1510
HVR HWB T6	640	990
LVR ISL T6	350	580
HVR HWB T3	300	460
LVR HEN T1	280	520
LVR HEN T5	280	520
HVR KIK T2	260	440
HVR BRY T7	250	430
HVR BRY T5	250	430
Constant EYR magnetic field		
Transformer	GIC [A](mean)	GIC [A](max)
HVR SDN T2	950	1590
LVR HEN T1	680	1160
LVR HEN T5	680	1160
LVR HWB T6	660	1100
HVR HEN T1	470	810
HVR HEN T5	470	810
HVR HWB T6	430	720
HVR SFD T10	360	610
HVR GLN T4	330	600
HVR GLN T5	330	600

Table 4: Top 10 transformers with the largest mean absolute GIC over a 60-minute interval during the three September 2017 extreme storm scenarios. The instantaneous one-minute time resolution maximum GIC is also given for those transformers.

Extreme storm based on September 2017		
ROGERS latitude variation		
Transformer	GIC [A](mean)	GIC [A](max)
HVR SDN T2	2100	4750
LVR HWB T6	1410	3170
HVR HWB T6	920	2070
HVR TWI T1	770	2270
HVR TWI T2	760	2250
LVR ISL T6	640	1490
HVR KIK T2	570	1350
HVR TIM T5	470	1120
HVR HWB T3	430	960
LVR ROX T10	370	830
NERC latitude variation		
Transformer	GIC [A](mean)	GIC [A](max)
HVR SDN T2	2210	4920
LVR HWB T6	1480	3280
HVR HWB T6	970	2130
HVR TWI T1	680	2130
HVR TWI T2	670	2120
LVR ISL T6	650	1490
HVR KIK T2	540	1280
LVR HEN T1	510	830
LVR HEN T5	510	830
HVR HWB T3	450	990
Constant EYR magnetic field		
Transformer	GIC [A](mean)	GIC [A](max)
HVR SDN T2	1770	3860
LVR HWB T6	1190	2600
LVR HEN T1	990	1770
LVR HEN T5	990	1770
HVR HWB T6	780	1690
LVR ISL T6	690	1570
HVR HEN T1	690	1220
HVR HEN T5	690	1220
HVR WRD T7	670	2190
HVR SFD T10	600	1150

Table 5: Top 30 transformers ranked by their 60-minute mean GIC for the nine extreme storm scenarios modeled. The right hand column is the mean for all the ranking; the smaller the number the higher the mean currents across the scenarios.

Transformers	1989 ROGERS	1989 ROGERS	1989 ROGERS	2003 NERC	2003 NERC	2003 NERC	2017 EYR	2017 EYR	2017 EYR	Mean rank
HVR SDN T2	1	1	1	1	1	1	1	1	1	1
LVR HWB T6	2	2	2	2	2	4	2	2	2	2.2
HVR HWB T6	3	3	5	3	3	7	3	3	5	3.9
LVR ISL T6	6	4	8	4	4	12	6	6	6	6.2
HVR KIK T2	7	7	11	8	8	14	7	7	12	9
LVR HEN T1	19	8	3	13	6	2	42	8	3	11.6
LVR HEN T5	20	9	4	14	7	3	43	9	4	12.6
HVR SFD T10	21	11	9	11	12	8	28	12	10	13.6
HVR HWB T3	9	10	27	5	5	20	9	10	28	13.7
HVR TIM T5	8	12	26	9	11	24	8	11	23	14.7
HVR BRY T7	10	13	21	6	9	15	18	19	24	15
HVR TWI T1	4	5	19	36	22	33	4	4	16	15.9
HVR BRY T5	11	14	22	7	10	16	19	20	25	16
HVR TWI T2	5	6	20	37	25	34	5	5	17	17.1
LVR TIM T5	14	18	34	12	14	30	17	24	33	21.8
HVR TKB T2	12	25	32	20	23	31	11	21	31	22.9
HVR TKB T3	13	26	33	21	24	32	12	22	32	23.9
HVR HEN T1	47	16	6	38	16	5	57	25	7	24.1
HVR HEN T5	48	17	7	39	17	6	58	26	8	25.1
HVR MAN T1	15	21	50	16	18	52	13	15	47	27.4
HVR MAN T5	16	22	51	17	19	53	14	16	48	28.4
LVR CML T8	22	19	47	10	13	36	26	27	59	28.8
HVR MAN T6	17	23	52	18	20	54	15	17	49	29.4
LVR ROX T10	29	30	60	15	15	38	10	14	56	29.7
HVR RDF T1	49	20	12	40	46	18	45	28	11	29.9
HVR MAN T7	18	24	53	19	21	55	16	18	50	30.4
HVR OHA T4	23	33	41	23	27	42	22	31	38	31.1
HVR OHA T5	24	34	42	24	28	43	23	32	39	32.1
LVR TIM T8	27	31	48	22	26	39	21	35	43	32.4
HVR RDF T3	50	27	13	41	53	21	46	29	14	32.7